Dalton Transactions

Magnetically Isolated Cuprate Spin-Ladder System: Synthesis, Structures, and Magnetic Properties

Journal:	*Dalton Transactions*
Manuscript ID:	DT-ART-06-2014-001746
Article Type:	Paper
Date Submitted by the Author:	12-Jun-2014

Complete List of Authors:	Zhang, Xiao; Hiroshima University, Department of Chemistry Nishihara, Sadafumi; Hiroshima University, Department of Chemistry Nakano, Yuki; Hiroshima University, Department of Chemistry Yoshida, Erina; Hiroshima University, Department of Chemistry Kato, Chisato; Hiroshima University, Department of Chemistry Ren, XiaoMing; College of Science, Nanjing University of Technology, Maryunina, Kseniya; Hiroshima University, Department of Chemistry Inoue, Katsuya; Hiroshima University, Department of Chemistry

Graphical and textual abstract for the table of contents

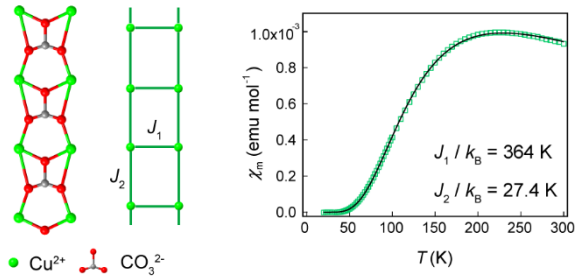

Two magnetically isolated cuprate spin ladder have been synthesized. Their crystal structures, and preliminary investigation into the magnetic properties were reported.

Journal Name

RSCPublishing

ARTICLE

Magnetically Isolated Cuprate Spin-Ladder System: Synthesis, Structures, and Magnetic Properties

Cite this: DOI: 10.1039/xoxxoooooox

Xiao Zhang,[a] Sadafumi Nishihara,*[a,b] Yuki Nakano,[a] Erina Yoshida,[a] Chisato Kato,[a] Xiao-Ming Ren,[c] Kseniya Yu. Maryunina,[a] Katsuya Inoue*[a,b]

Received ooth January 2012,
Accepted ooth January 2012

DOI: 10.1039/xoxxoooooox

www.rsc.org/

We synthesized and characterized two magnetically isolated spin ladders, $Cu_2(CO_3)(ClO_4)_2(NH_3)_6$ (**1**) and $Cu_2(CO_3)(ClO_4)_2(H_2O)(NH_3)_5$ (**2**), which are the first examples of carbonate bridging molecular spin ladders. Compounds **1** and **2** form a ladder configuration by stacking a structural unit composed of two Cu^{2+} ions and one CO_3^{2-}, where the Cu–O–Cu interactions form the rungs and legs of each ladder and the counter anions (ClO_4^-) occupy the space between the ladders and ensure their magnetic isolation. A $S = 1/2$ magnetically isolated spin-ladder model with a ladder-rung magnetic interaction $J_1/k_B = 364$ K (where J is defined as positive for antiferromagnetic interactions) and a ladder-leg magnetic interaction $J_2/k_B = 27.4$ K accurately predicts the temperature dependence of the molar magnetic susceptibility for **1**. The ladder configuration of **2** is similar to that of **1** except that the CO_3^{2-} is alternately skewed in different directions in the stacked structural unit. Interestingly, this minor structural variation in **2** results in its remarkably different magnetic behavior; the magnetic susceptibility curve of **2** is accurately described by an alternating chain model with $J_3/k_B = 7.26$ K and $J_4/k_B = 4.42$ K.

Introduction

Understanding the mechanism of superconductivity can have a significant impact in the fields of condensed-matter physics and material science. Among the various superconductors discovered,[1-11] cuprate superconductors are the most exciting materials and have been extensively studied because of their high critical temperature (T_c). High-T_c superconductivity in these materials is attributed to the characteristic two-dimensional CuO_2 sheet structure with doped carriers.[3,4]

The simplest form of the CuO_2 sheet structure, i.e., spin-ladder system obtained by shearing CuO_2 sheets,[12-15] has attracted significant attention. Spin ladders are a family of quasi-one-dimensional magnetic systems composed of odd or even numbers of antiferromagnetic Heisenberg chains, which are antiferromagnetically coupled to each other. Theoretical calculations[13-15] and experimental results[16-19] show that odd-leg spin ladders are gapless and exhibit properties similar to those of an antiferromagnetic Heisenberg chain. Meanwhile, even-leg spin ladders have a spin-liquid ground state with a finite spin gap (Δ) and exhibit superconductivity when hole doped.

Only a few cuprate inorganic spin ladders have been studied, such as $(Sr, Ca)_{14}Cu_{24}O_{41}$,[6,20] $Sr_{n-1}Cu_{n+1}O_{2n}$ (n = 3, 5),[16-19] and $LaCuO_{2.5}$.[21,22] The widely studied spin ladder $(Sr, Ca)_{14}Cu_{24}O_{41}$ is composed of stacks of CuO_2 chain layers and Cu_2O_3 two-leg ladder layers. Ladders formed by Cu–O–Cu bond angles of 180º build up a strong intra-ladder antiferromagnetic interaction by the superexchange path, while inter-ladder coupling is very weak because of weak ferromagnetic interaction due to Cu–O–Cu bond angles of 90º. Since the average valence of Cu is +2.25, such a compound is intrinsically doped with holes. Extensive conductivity studies have led to the realization of theoretically predicted superconducting T_c of 12 K and 9 K under high pressures of 3.0 GPa and 4.5 GPa, respectively.[6] However, the hole doped two-leg spin ladder, $(La,Sr)CuO_{2.5}$, does not show superconductivity even at high pressures.[22,23] In this case, the absence of superconductivity can be attributed to strong inter-ladder interactions.[24-26] An ideal spin ladder, i.e., a ladder without inter-ladder interactions, is therefore essential for studies on the superconductivity mechanism in spin ladders.

Molecular spin ladders[27-33] attract significant attention in this regard, as the expected weak inter-ladder interactions allow for them to be considered as isolated ladders. For example, the molecular spin ladder $[(DT\text{-}TTF)_2][Au(mnt)_2]$ (DT-TTF = dithiophentetrathiafulvalene, mnt = maleonitriledithiolate), with segregated regular stacks of $[(DT\text{-}TTF)_2]^+$ and $[Au(mnt)_2]^-$, has been reported.[34-35] The stack of side-by-side pair of donor cations, $[(DT\text{-}TTF)_2]^+$, forms the two chains that become constitute the legs in the ladder structure along the stacking direction. These two chains are strongly linked by inter-chain S•••S contacts, which define the ladder rungs. Meanwhile, single stacks of diamagnetic $[Au(mnt)_2]^-$ alternate with the $[(DT\text{-}TTF)_2]^+$ ladder, weakening the inter-ladder interactions, and hence, the ladder can be considered as an isolated spin ladder. Similarly, other examples of molecular spin ladders formed by molecular assembly include *p*-EPYNN-Ni(dmit)$_2$ (*p*-EPYNN = *p*-N-ethylpyridinium α-nitronylnitroxide, $dmit_2^-$= 2-thioxo-1,3-dithiole-4,5-dithiolate),[36,37] and $[Ph(NH_3)]$([18]crown-6)$[Ni(dmit)_2]$,[38-42] wherein the π–π overlap and S•••S contacts provide the intra-ladder interactions,

Table 1. Crystallographic data for $Cu_2(CO_3)(ClO_4)_2(NH_3)_6$ (**1**) and $Cu_2(CO_3)(ClO_4)_2(H_2O)(NH_3)_5$ (**2**).

Compound	**1**	**2** (HT phase)	**2** (LT phase)
Formula	$CH_{18}Cl_2N_6O_{11}Cu_2$	$CH_{17}Cl_2N_5O_{12}Cu_2$	$CH_{17}Cl_2N_5O_{12}Cu_2$
Formula weight	488.19	489.17	489.17
Temperature (K)	173 (2)	296 (2)	100 (2)
Crystal system	Orthorhombic	Orthorhombic	Orthorhombic
Space group	*Pbam*	*Pnma*	*Pnma*
a (Å)	9.277(3)	9.8827(5)	9.8063(6)
b (Å)	17.304(6)	15.1534(7)	15.1247(9)
c (Å)	4.7930(17)	10.0629(5)	9.8609(6)
V (Å^3)	769.4(5)	1506.98(13)	1462.54(15)
Z	2	4	4
$R1$, $\omega R2$ [$I > 2\sigma(I)$]	0.0617, 0.1509	0.0284, 0.0717	0.0285, 0.0672
$R1$, $\omega R2$ indices (all data)	0.0666, 0.1539	0.0408, 0.0794	0.0380, 0.0713
GOF	1.017	1.082	1.164

and the arrangement of cations between the ladders reduces the inter-ladder interactions. However, these molecular spin ladders, which rely on weak intermolecular forces for their structure, cannot sustain their configuration when doped. In fact, successful doping in a molecular spin ladder has not been reported so far.

The construction of a cuprate spin ladder without inter-ladder interactions is, therefore, a critical task for studying the mechanism of high-T_c superconductivity. In this study, we describe the synthesis of two such magnetically isolated spin-1/2 ladders with copper cations (Cu^{2+}) and carbonate anions (CO_3^{2-}). The synthesized spin ladders—$Cu_2(CO_3)(ClO_4)_2(NH_3)_6$ (**1**) and $Cu_2(CO_3)(ClO_4)_2(H_2O)(NH_3)_5$ (**2**)—contain perchlorate anions (ClO_4^-) between the ladders, which ensure the isolation of ladders. The structure and preliminary investigations into the magnetic properties of **1** and **2** are reported.

Experimental Section

Synthesis.

$Cu_2(CO_3)(ClO_4)_2(NH_3)_6$ (**1**): Compound **1** was synthesized by mixing solutions of $CuCO_3$•$Cu(OH)_2$ (0.032 mmol in 20% aqueous ammonia (3 mL)) and $Cu(ClO_4)_2$•$6H_2O$ (0.32 mmol in ethanol (4 mL)) at room temperature. Slow evaporation over two days led to the formation of light blue single crystals of **1**. Found: C, 2.60; H, 3.82; N, 17.03. Calc. for $CH_{18}Cl_2N_6O_{11}Cu_2$: C, 2.46; H, 3.72; N, 17.21%. IR (KBr pellet, cm^{-1}): 3320, 3233, 3168, 1620, 1521, 1471, 1370, 1243, 1143, 1120, 1089, 636, and 627.

$Cu_2(CO_3)(ClO_4)_2(H_2O)(NH_3)_5$ (**2**): Compound **2** was synthesized by mixing solutions of $CuCO_3$•$Cu(OH)_2$ (2 mmol in 20% aqueous ammonia (25 mL)) and $Cu(ClO_4)_2$•$6H_2O$ (2 mmol in a mixture of ethanol (16.5 mL) and water (8.5 mL)) under an atmosphere of carbon dioxide at room temperature. Slow evaporation over two weeks led to the formation of dark blue single crystals of **2**. Found: C, 2.55; H, 3.46; N, 14.61. Calc. for $CH_{17}Cl_2N_5O_{12}Cu_2$: C, 2.46; H, 3.50; N, 14.32%. IR (KBr pellet, cm^{-1}): 3446, 3313, 3165, 1615, 1400, 1257, 1145, 1120, 1089, 636, and 628.

X-ray Crystallography.

Diffraction data for crystals of **1** and **2** were collected on a Bruker SMART APEX II CCD diffractometer with graphite-monochromated Mo Kα radiation, $\lambda = 0.71073$ Å.

The single crystal of **1** was mounted in a stream of cold nitrogen gas and measured at 173 K. In case of **2**, to study phase transitions, a single crystal was measured both at room temperature and 100 K to determine high-temperature (HT) and low-temperature (LT) phases, respectively. Numerical and empirical absorption corrections were applied to data collected from **1** and **2**, respectively. The structures were solved via direct methods by SIR 97 and refined by least squares using SHELX-97. The isotropically refined hydrogen atoms of ammonia were placed at calculated positions, and the positions of hydrogen atoms of water were not defined. Crystallographic details and data collection parameters for **1** and **2** are given in Table 1.

DSC Measurements.

Phase transition in **2** was analyzed by differential scanning calorimetry (DSC) measurements (DSC 8230, Rigaku Inc.) from 160 K to 250 K using a temperature sweep rate of ±5 K min^{-1}.

Magnetic Susceptibility Measurements.

The magnetic susceptibility measurement data for **1** and **2** were collected using a superconducting quantum interference device (SQUID) magnetometer (MPMS-5S, Quantum Design, Inc.). The temperature dependence of the molar magnetic susceptibilities was measured in an applied magnetic field of 5,000 Oe for **1** and 10,000 Oe for **2**. For **2**, additional measurements were conducted by increasing and decreasing temperature between 195 K and 215 K with a finer temperature step.

Results and discussion

Structures.

Compound **1** adopts the orthorhombic *Pbam* space group. The observed ladder structure in **1** is disordered; one ladder overlaps with another oppositely orientated crystallographically equivalent ladder (Fig. S1, Supporting Information). One of the two disordered ladders is depicted in Fig. 1a; this ladder is formed by stacking a structural unit composed of two Cu^{2+} ions with coordinated ammonium molecules (NH_3) and one CO_3^{2-}. The thermal ellipsoid plot (50% probability level) of the partial structure of the ladder with the atom labeling scheme is shown in Fig. 1b. Crystallographically independent Cu1 is hexa-coordinated; three oxygen atoms of CO_3^{2-} and three nitrogen atoms of NH_3 coordinate with Cu1 in a distorted octahedral arrangement with Cu–O and Cu–N bond lengths of 2.001–2.833 Å and 2.016–2.025 Å, respectively. In this structure, the axis elongated by the Jahn–Teller effect is aligned along the ladder leg (O6(a)–Cu1(a)–O6(c) and crystallographically equivalent O6(b)–Cu1(b)–O6(d); see Fig. 1b).

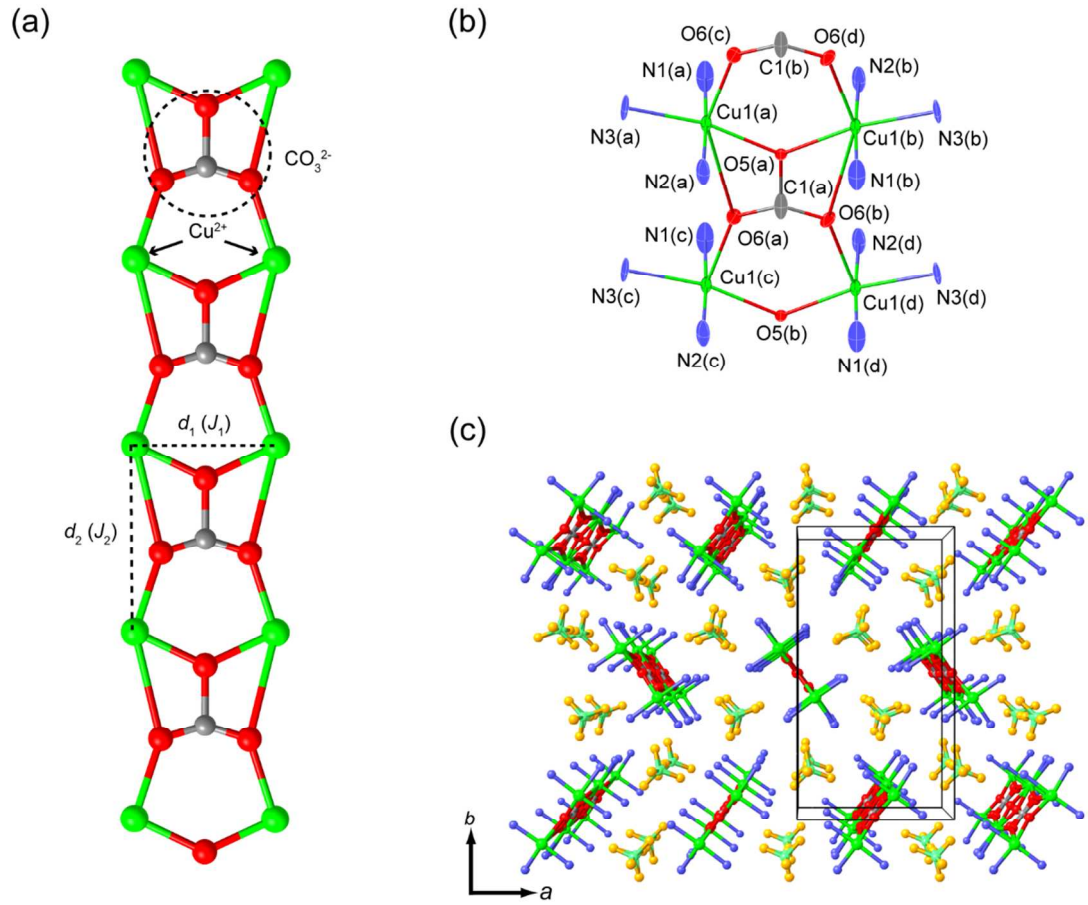

Figure 1. Crystal structures of $Cu_2(CO_3)(ClO_4)_2(NH_3)_6$ (**1**): (a) the ladder structure formed by the stacking of a structural unit composed of two Cu^{2+} ions and one CO_3^{2-} along the *c*-axis. The ammonium molecules coordinating to Cu^{2+} ions are hidden for clarity; (b) thermal ellipsoid plot (50% probability) of the partial structure of the ladder with the atom numbering scheme; and (c) perspective view of the crystal structure along the *c*-axis (the ladder leg direction).

Next, we focus on the CO_3^{2-} motif, which bridges the Cu^{2+} ions and configures the cuprate spin ladder. The oxygen atom O5 links two Cu1 (Cu1(a)–O5(a)–Cu1(b); see Fig. 1b), forming the rung feature of the ladder. In addition, another oxygen, O6(a), bonds to Cu1(a) and Cu1(c), a feature that is crystallographically equivalent to that of Cu1(b)–O6(b)–Cu1(d), which forms the ladder-leg configuration. As a result, two distinct distances observed between adjacent Cu^{2+} ions along the ladder rung and leg are d_1 = 3.622 Å and d_2 = 4.793 Å, respectively (Fig. 1a).

Fig. 1c depicts the packing structure of **1** viewed along the *c*-axis (the ladder leg direction), showing the geometry of the stacked ladders. The strong inter-ladder interactions promote magnetic ordering in the ground state of a spin ladder, e.g., in the compound $LaCuO_{2.5}$.[21-26] In $LaCuO_{2.5}$, strong inter-ladder interactions are observed owing to the presence of Cu–O–Cu inter-ladder coordination bonds. By contrast, a ladder in **1** is not coordinately connected to another ladder. In addition, uncoordinated counter anions ClO_4^-, located between the ladders, separate the ladders by 7.4 Å, further ensuring that each ladder is magnetically isolated.

Single-crystal X-ray diffraction measurements of **2** at room temperature (HT) and 100 K (LT) reveal that the compound belongs to the orthorhombic *Pnma* space group, irrespective of the temperature. Even though the crystal structure of the HT phase is similar to that of the LT phase, the results of magnetic susceptibility (Fig. S2, Supporting Information), DSC (Fig. S3, Supporting Information), and ESR measurements (Fig. S4, Supporting Information) indicate that there is a structural first order phase transition taking place at ~205K. Such phase transitions have been frequently reported for coordination compounds and involve the conversion of the equatorial and axial positions on the Cu^{2+} ion.[43,44]

The ladder structure of the LT phase is depicted in Fig. 2a, and a thermal ellipsoid plot (50% probability level) of the partial structure of the distorted ladder with the atom numbering scheme is shown in Fig. 2b. The ladder structure of **2** has Cu^{2+} ions coordinated to NH_3 and H_2O in two distinct environments. In one setting, Cu^{2+} (Cu1) forms a distorted octahedral geometry with three oxygen atoms from CO_3^{2-} and three nitrogen atoms from NH_3, where the Cu–O and Cu–N bond lengths are 2.003–2.622 Å and 2.005–2.034 Å, respectively, and the axis elongated by the Jahn–Teller effect is along the ladder leg (O1(a)–Cu1(a)– O2(b); see Fig. 2b). The other Cu^{2+} (Cu2) forms a penta-coordinated pyramidal geometry with two oxygen atoms from CO_3^{2-}, two nitrogen atoms from NH_3 molecules, and one water molecule, wherein the Cu–O and Cu–N bond lengths are 1.946–2.221 Å and 1.991 Å, respectively, and the elongation of axis by the Jahn–Teller effect is observed along the rung of the ladder (Cu2(a)–O3(a); See Fig. 2b).

The ladder configuration in **1** is slightly different from that in **2**. In **1**, a symmetric unit is composed of two Cu^{2+} ions and one CO_3^{2-} stacked along the ladder leg, while in **2**, the structural unit is composed of two Cu^{2+} ions and a skewed CO_3^{2-} stacked along the ladder leg. In **2**, the CO_3^{2-} is skewed alternately in

two different directions; consequently, alternating bonds between Cu^{2+} and an oxygen along the ladder leg are broken

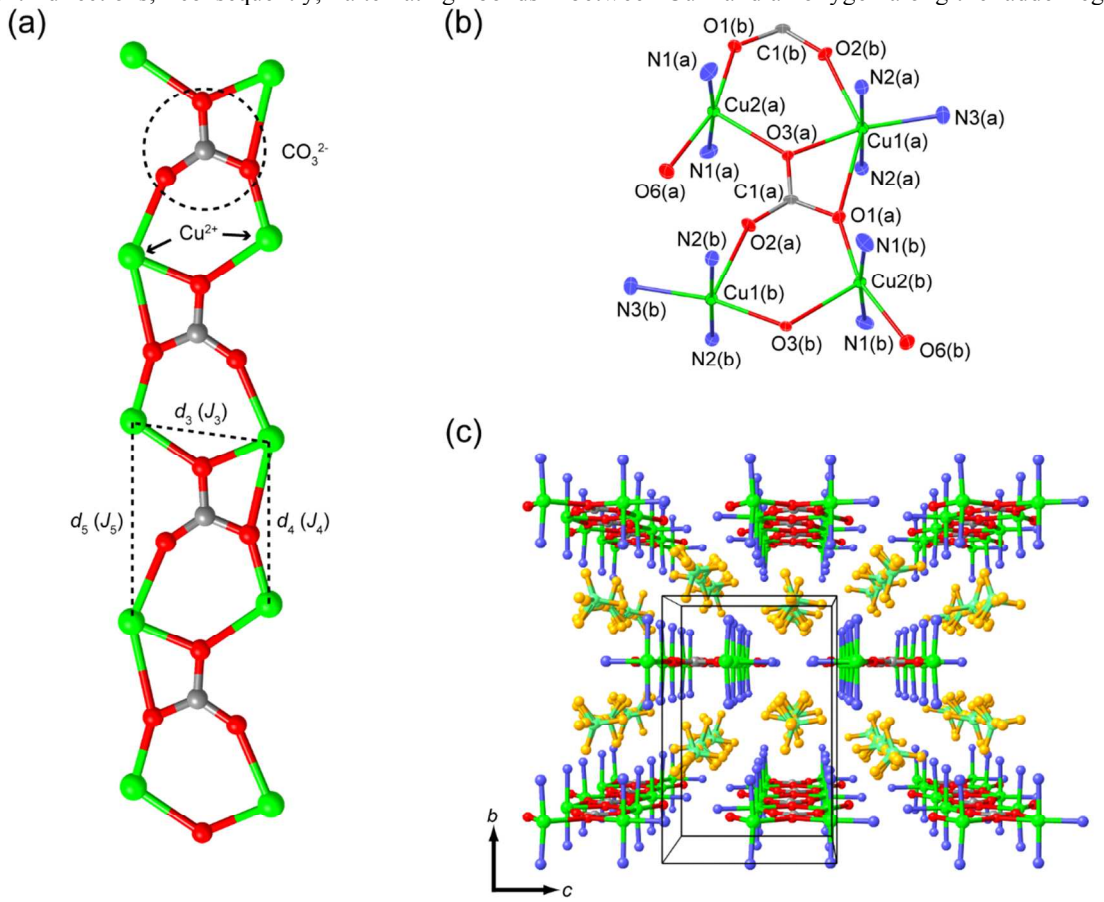

Figure 2. Crystal structures of $Cu_2(CO_3)(ClO_4)_2(H_2O)(NH_3)_5$ (**2**): (a) the distorted ladder configured by the stacking of the asymmetric unit composed of two Cu^{2+} ions and one CO_3^{2-} along the *a*-axis. The ammonium and water molecules coordinating to Cu^{2+} ions are hidden for clarity; (b) thermal ellipsoid plot (50% probability level) of the partial structure of the ladder with the atom numbering scheme; and (c) perspective view of the crystal structure along the *a*-axis (the ladder leg direction).

(e.g., Cu2(a)–O2(a); see Fig. 2b). The distances between adjacent Cu^{2+} ions in **2** are d_3 = 3.717 Å along the rung of the ladder and d_4 = 4.430 Å and d_5 = 5.377 Å along the ladder leg (Fig. 2a). Fig. 2c is a perspective view of the crystal structure of **2** along the *a*-axis (the ladder leg direction) showing the geometrical stacks of distorted ladders. The counter anions (ClO_4^-) are situated between the ladders, and the shortest distance between the adjacent ladders is estimated to be 6.2 Å.

Magnetic Properties.

The temperature-dependent molar magnetic susceptibility, χ_m, of **1** measured at 5000 Oe is shown in Fig. 3, where contributions from temperature-independent magnetic components—e.g., a diamagnetic component of -8.01 × 10^{-5} emu mol^{-1}—are subtracted. The instability of crystals of **1** during long periods of exposure to air results in increased Curie component, which can be attributed to the paramagnetic impurities. Note that to aid accurate analysis, molar magnetic susceptibilities of **1** at temperatures <20 K are not included in Fig. 3 (Fig. S5 shows the extended data). With decrease in temperature, the value of χ_m initially increases gradually, showing a broad peak with its maxima at ~220 K (typical of low-dimensional antiferromagnetic compounds), and subsequently decreases exponentially with a finite spin gap. At low temperatures (<50 K), a prominent Curie tail is observed.

The temperature dependence of molar magnetic susceptibility of **1** is modeled according to the following Hamiltonian:

$$H = J_1 \sum_i^{N/2} \boldsymbol{S}_{1,i} \cdot \boldsymbol{S}_{2,i} + J_2 \sum_i^{N/2} \left(\boldsymbol{S}_{1,i} \cdot \boldsymbol{S}_{1,i+1} + \boldsymbol{S}_{2,i} \cdot \boldsymbol{S}_{2,i+1} \right) \quad (1)$$

where J_1 and J_2 are the exchange magnetic interactions that link spin operator $\boldsymbol{S}_{n,i}$ along the ladder rung and leg, respectively, and J is defined as positive (negative) for antiferromagnetic (ferromagnetic) interactions. All experimentally measured magnetic susceptibility values for temperatures >20 K were fitted to the S = 1/2 magnetically isolated spin-ladder model[45] with a Curie term C_{imp}/T,

$$\chi = \frac{N g^2 \beta^2}{J_1} \frac{e^{-\Delta^*_{fit}/t}}{4t} P^{(p)}_{(q)}(t) + \frac{C_{imp}}{T}, \quad (2)$$

with four independent variables: ladder-rung magnetic interaction J_1 (see Fig. 3), ladder-leg magnetic interaction J_2 (see Fig. 3), g, and C_{imp} (which is the Curie contribution owing to paramagnetic impurities; details of eq. 2 are provided in Supporting Information). The resulting good fit (see Fig 3, blue solid line) with J_1/k_B = 364 K, J_2/k_B = 27.4 K, g = 2.23, and C_{imp} = 0.00660 emu K mol^{-1} suggests that the magnetic structure is an ideal magnetically isolated spin ladder. It is noted that the results of the fitting slightly change depending on the impurity concentrations (see Fig. S6-S8). The spin gap can be calculated to be Δ/k_B = 338 K from the theoretical equation,[46]

$$\Delta = J_1 - J_2 + {J_2}^2/2J_1 \qquad (3)$$

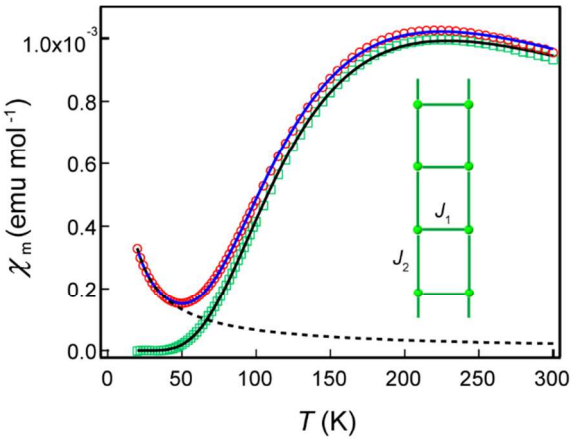

Figure 3. Temperature-dependent molar magnetic susceptibilities of $Cu_2(CO_3)(ClO_4)_2(NH_3)_6$ (**1**, red circles). The blue solid line represents the fit according to eq. 2 (see text). The green open squares and black solid line show the molar magnetic susceptibilities of the spin-ladder component after subtracting the estimated contributions from the Curie component (black dashed line) and the fitting by eq. 2 without the Curie component, respectively. Inset: schematic representation of the ladder configuration in **1** with ladder-rung (J_1) and ladder-leg (J_2) magnetic interactions.

using the estimated values for magnetic interactions J_1 and J_2.

The molar magnetic susceptibilities of **2** measured from 300 K to 2 K under 10000 Oe are shown in Fig. 4. Contributions from the temperature-independent magnetic component (-3.80×10^{-5} emu mol^{-1}) have been subtracted from the data. With decrease in temperature, the χ_m values gradually increase in accordance with the Curie law. After showing a peak at ~4 K, the values decrease because of the magnetic interaction between Cu^{2+} ions. We reinvestigated the molar susceptibility of **2** in the 195 - 215 K temperature range with a finer temperature step to study the phase transition. The observed weak hysteresis in susceptibility data of HT and LT phases (Fig. S2) reveals that the phase transition in this region influences the magnetic behavior of **2**.

Attempts to fit the susceptibility data obtained from **2** with the aforementioned $S = 1/2$ magnetically isolated spin-ladder model (eq. 2) and with the assumption that $J_4 = J_5$ (Fig. 4) are unsuccessful, indicating that one of the ladder-leg magnetic interaction (J_5) is significantly smaller than the other (J_4). Therefore, eq. 5 ignores the contribution of J_5 and is composed of a Curie term C_{imp}/T (due to impurities) and an alternating chain model based on the following Hamiltonian (eq. 4),[47]

$$H = J\sum_{i=1}^{N/2}[\boldsymbol{S}_{2i}\cdot\boldsymbol{S}_{2i-1} + \alpha\boldsymbol{S}_{2i}\cdot\boldsymbol{S}_{2i+1}] \qquad (4)$$

$$\chi = \frac{Ng^2\beta^2}{kT}\frac{A + Bx + Cx^2}{1 + Dx + Ex^2 + Fx^3} + \frac{C_{imp}}{T}, \qquad (5)$$

where α ($0 \le \alpha \le 1$) is the alternation parameter, $x = |J|/k_BT$, and the coefficients A–F are described in Supporting Information.

The best fit is obtained for $J_3/k_B = 7.26$ K, $J_4/k_B = 4.42$ K ($\alpha = 0.609$), $g = 2.20$, and $C_{imp} = 0.0180$ emu K mol^{-1}, which indicates that the magnetic configuration of **2** can be considered to be an antiferromagnetic Heisenberg chain with alternating exchange (see Fig. 4).

The widely employed Goodenough-Kanamori-Anderson rules estimate the magnetic interaction between two magnetic ions through a superexchange pathway,[48-50] wherein a 180° superexchange of two magnetic ions with partially filled d shells is strongly antiferromagnetic, while a 90° superexchange interaction is very weakly ferromagnetic. The magnetic interactions along the ladder rung in both our compounds are determined to be antiferromagnetic from magnetic susceptibility measurements, despite the fact that the Cu–O–Cu bond angle is close to 90° (Table S1, Table S2, Table S3, Supporting Information). Previous reports contain several similar examples of complexes composed of Cu^{2+} ions and CO_3^{2-}.[51-53]

A comparison of the magnitudes of magnetic interactions of ladder rung and leg in **1** indicates that the interaction along the ladder rung is significantly larger than that along the ladder leg. This large difference in the magnitude of the two interactions is considered to influence not only the distances between Cu^{2+} ions but also the coordination configuration of Cu–O–Cu. In the ladder structure of **1**, the octahedral geometry around Cu^{2+} ion is elongated along the ladder leg by the Jahn–Teller effect (O6(a)–Cu1(a)–O6(c) and O6(b)–Cu1(b)–O6(d); see Fig. 1b). As a result, the spin density in the d_{z2} orbital along the axial coordination site is very low, and the magnetic orbitals are nearly orthogonal to the d_{x2-y2} orbital. Consequently, the ladder-leg interaction through the superexchange pathway between axial sites (d_{z2}–d_{z2}) is significantly smaller than the ladder-rung interaction between magnetic orbitals (d_{x2-y2}–d_{x2-y2}). The estimated magnetic interactions in **1** are consistent with those reported for Cu^{2+} tetramer coordinated to CO_3^{2-}, which have a configuration similar to that of the structural unit of the ladder in **1**.[51-53]

Similar considerations for compound **2** reveal why the ladder-rung (J_3) and ladder-leg (J_4) magnetic interactions are of similar magnitudes, but weaker than ladder-rung interaction (J_1) in **1**. The Jahn–Teller effect on the octahedrally coordinated Cu^{2+} ion in **2** elongates the axis along the ladder leg (O1(a)–Cu1(a)–O2(b); see Fig. 2b), while a similar effect on pyramidally coordinated Cu^{2+} ions elongates the axis along the ladder rung (Cu2(a)–O3(a); see Fig. 2b). Therefore, magnetic interactions in ladder rung and leg in **2** occur through a weak superexchange pathway between axial and equatorial orbitals.

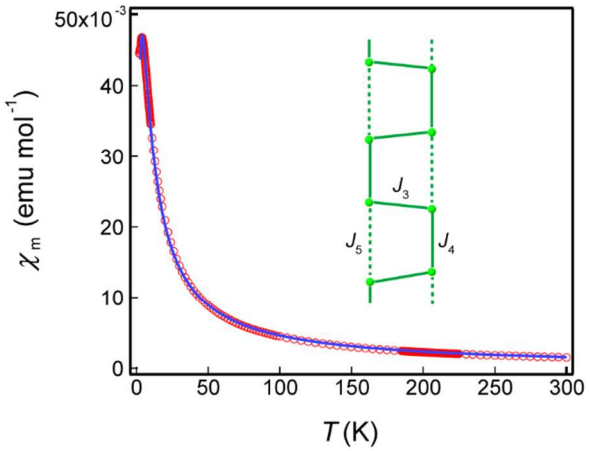

Figure 4. Temperature dependence of molar magnetic susceptibility of $Cu_2(CO_3)(ClO_4)_2(H_2O)(NH_3)_5$ (**2**, red circles). The blue solid line represents the fit provided by eq. 5 (see text). Inset: schematic representation of the distorted ladder configuration in **2** with the ladder-rung (J_3) and two different ladder-leg (J_4 and J_5) magnetic interactions.

Conclusions

In conclusion, we report the synthesis, crystal structures, and preliminary investigation into the magnetic properties of $Cu_2(CO_3)(ClO_4)_2(NH_3)_6$ (**1**) and $Cu_2(CO_3)(ClO_4)_2(H_2O)(NH_3)_5$ (**2**), which are the first examples of carbonate bridging compounds presenting a magnetically isolated spin ladder. Compound **1** attains the ladder configuration as a result of stacking of a structural unit composed of two Cu^{2+} ions and one CO_3^{2-}, where Cu–O–Cu contacts form the legs and rungs of the ladder. The ClO_4^- counter anions, located in the space between the ladders, ensure that the spin ladders are magnetically isolated from each other. The temperature dependence of molar magnetic susceptibility can be accurately predicted by the S = 1/2 magnetically isolated spin-ladder model with J_1/k_B = 364 K and J_2/k_B = 27.4 K for the ladder-rung and leg interaction, respectively. Compound **2** has a ladder configuration similar to that in **1**, except that CO_3^{2-} in the unit structure is skewed, thereby creating two asymmetric unit structures that are stacked alternately to form the ladder configuration. This minor structural distinction between the two spin ladders leads to their remarkably different magnetic behavior, wherein the magnetic susceptibility curve of **2** is predicted by an alternating chain model with J_3/k_B = 7.26 K and J_4/k_B = 4.42 K.

These compounds possess the benefits of both inorganic and molecular spin ladders, i.e., they possess a rigid structure and may be able to sustain the ladder structure when carrier-doped, as in the case of inorganic compounds, and form magnetically isolated spin ladders, as in the case of molecular spin ladders. These compounds, therefore, demonstrate huge potential as excellent model two-leg antiferromagnetic spin ladders and for unrealized molecular spin-ladder superconductors.

Acknowledgements

This study was supported by the Japan Society for Promotion of Science (JSPS) through KAKENHI Grant Numbers 24350095, 23655178, and 25220803. We also acknowledge the support of the Cooperative Research Program of "Network Joint Research Center for Materials and Devices," the 2010 Hiroshima University Fujii Research Promotion Fund, Hitachi Metals & Materials Science Foundation, and Murata Science Foundation, Japan.

Notes and references

[a] Department of Chemistry, Hiroshima University, Higashi-hiroshima 739-8526, Japan. Fax: +81 82 424 7418; E-mail: snishi@hiroshima-u.ac.jp.

[b] Institute for Advanced Materials Research, Hiroshima University, Higashi-hiroshima 739-8530, Japan

[c] College of Science, Nanjing University of Technology, Nanjing 210009, P. R. China, and State Key Lab & Coordination Chemistry Institute, Nanjing University, Nanjing 210093, P. R. China.

Electronic Supplementary Information (ESI) available: CCDC reference numbers CCDC-1003017 and 1003018. See DOI: 10.1039/b000000x/

1 H. K. Onnes, *Commun. Phys. Lab. Univ. Leiden. Suppl*. 29 (Nov. 1911).

2 W. Meissner, *Mitteilung*, 1929, 571.

3 J. G. Bednorz, K. A. Müller, *Z. Phys. B* 1986, **64**, 189.

4 M. K. Wu, J. R. Ashburn, C. J. Torng, P. H. Hor, R. L. Meng, L. Gao, Z. J. Huang, Y. Q. Wang, C. W. Chu, *Phys. Rev. Lett*. 1987, **58**, 908.

5 J. Nagamatsu, N. Nakagawa, T. Muranaka, Y. Zenitani, J. Akimitsu, *Nature* 2001, **410**, 63.

6 M. Uehara, T. Nagata, J. Akimitsu, H. Takahashi, N. Môri, K. Kinoshita, *J. Phys. Soc. Jpn*. 1996, **65**, 2764.

7 Y. Kamibara, T. Watanabe, M. Hirano, H. Hosono, *J. Am. Chem. Soc*. 2008, **130**, 3296.

8 D. Jérome, A. Mazaud, M. Ribault, K. Bechgaard, *J. Phys. Lett*. (Paris) 1980, **41**, L95.

9 R. L. Greene, E. M. Engler, *Phys. Rev. Lett*. 1980, **45**, 1587.

10 H. Urayama, H. Yamochi, G. Saito, K. Nozawa, T. Sugano, M. Kinoshita, S. Sato, K. Oshima, A. Kawamoto, J. Tanaka, *Chem. Lett*. 1988, **17**, 55.

11 A. F. Hebard, M. J. Rosseinsky, R. C. Haddon, D. W. Murphy, S. H. Glarum, T. T. M. Palstra, A. P. Ramirez, A. R. Kortan, *Nature* 1991, **350**, 600.

12 P. W. Anderson, *Science* 1987, **235**, 1196.

13 E. Dagotto, J. Riera, D. Scalapino, *Phys, Rev. B* 1992, **45**, 5744.

14 T. M. Rice, S. Gopalan, M. Sigrist, *Europhys. Lett*. 1993, **23**, 445.

15 E. Dagotto, T. M. Rice, *Science* 1996, **271**, 618.

16 M. Azuma, Z. Hiroi, M. Takano, K. Ishida, Y. Kitaoka, *Phys. Rev. Lett*. 1994, **73**, 3463.

17 K. Ishida, Y. Kitaoka, K. Asayama, M. Azuma, Z. Hiroi, M. Takano, *J. Phys. Soc. Jpn*. 1994, **63**, 3222.

18 M. Azuma, H. Yoshida, T. Saito, T. Yamada, M. Takano, *J. Am. Chem. Soc*. 2004, **126**, 8244.

19 K. Kojima, A. Keren, G. M. Luke, B. Nachumi, W. D. Wu, Y. J. Uemura, M. Azuma, M. Takano, *Phys. Rev. Lett*. 1995, **74**, 2812.

20 E. M. McCarron, M. A. Subramanian, J. C. Calabrese, R. L. Harlow, *Mat. Res. Bull*. 1988, **23**, 1355.

21 R. J. Cava, T. Siegrist, B. Hessen, J. J. Krajewski, W. F. Peck, B. Batlogg, H. Takagi, J. V. Waszczak, L. F. Schneemeyer, H. W. Zandbergen, *Physica C* 1991, **177**, 115.

22 Z. Hiroi, M. Takano, *Nature* 1995, **377**, 41.

23 T. Nakanishi, N. Móri, C. Murayama, H. Takanashi, T. Nagata, M. Uehara, J. Akimitsu, K. Kinoshita, N. Motoyama, H. Eisaki, S. Uchida, *J. Phys. Soc. Jpn*. 1998, **67**, 2408.

24 M. Troyer, M. E. Zhitomirsky, K. Ueda, *Phys. Rev. B* 1997, **55**, 6117.

25 S. Matsumoto, Y. Kitaoka, K. Ishida, K. Asayama, Z. Hiroi, N. Kobayashi, M. Takano, *Phys. Rev. B* 1996, **53**, R11942.

26 R. Kadono, H. Okajima, A. Yamashita, K. Ishii, T. Yokoo, J. Akimitsu, N. Kobayashi, Z. Hiroi, M. Takano, K. Nagamine, *Phys. Rev. B* 1996, **54**, R9628.

27 N. Robertson, L. Cronin, *Coord. Chem. Rev*. 2002, **227**, 93.

28 C. Rovira, *Chem. Eur. J*. 2000, **6**, 1723.

29 B. R. Paryal, B, L. Scott, R. D. Willett, *Phys. Rev. B* 1990, **41**, 1657.

30 B. Chiari, O. Piovesana, T. Tarantelli, P. F. Zanazzi, *Inorg. Chem.* 1990, **29**, 1172.

31 A. Shapiro, C. P. Landee, M. M. Turnbull, J. Jornet, M. Deumal, J. J. Novoa, M. A. Robb, W. Lewis, *J. Am. Chem. Soc*. 2007, **129**, 952.

32 F. Awwadi, R. D. Willett, B. Twamley, R. Schneider, C. P. Landee, *Inorg. Chem.* 2008, **47**, 9327.

33 R. D. Willett, C. Galeriu, C. P. Landee, M. M. Turnbull, B. Twamley, *Inorg. Chem.* 2004, **43**, 3804.

34 C. Rovira, J. Veciana, E. Ribera, J. Tarrés, E. Canadell, R. Rousseau, M. Mas, E. Molins, M. Almeida, R. T. Henriques, J. Morgado, J.–P. Schoeffel, J.–P. Pouget, *Angew. Chem. Int, Ed*. 1997, **36**, 2324.

35 D. Arčon, A. Lappas, S. Margadonna, K. Prassides, E. Ribera, J. Veciana, C. Rovira, R. T. Henriques, M. Almeida, *Phys. Rev. B* 1999, **60**, 4191.

36 H. Imai, T. Inabe, T. Otsuka, T. Okuno, K. Awaga, *Phys. Rev. B* 1996, **54**, R6838.

37 H. Imai, T. Otsuka, T. Naito, K. Awaga, T. Inabe, *J. Am. Chem. Soc*. 1999, **121**, 8098.

38 S. Nishihara, T. Akutagawa, T. Hasegawa, T. Nakamura, *Chem. Commun*. 2002, 408.

39 S. Nishihara, T. Akutagawa, T. Hasegawa, S. Fujiyama, T. Nakamura, T. Nakamura, *J. Solid State Chem*. 2002, **168**, 661.

40 S. Nishihara, T. Akutagawa, T. Hasegawa, T. Nakamura, S. Fujiyama, T. Nakamura, *Synth. Met*. 2003, **137**, 1279.

41 S. Nishihara, T. Akutagawa, D. Sato, S. Takeda, S. Noro, T. Nakamura, *Chem. Asian. J*. 2007, **2**, 1083.

42 S. Nishihara, X. Zhang, K. Kunishio, K. Inoue, X. M. Ren, T. Akutagawa, J. I. Kishine, M. Fujisawa, A. Asakura, S. Okubo, H. Ohta, T. Nakamura, *Dalton Trans*. 2013, **42**, 15263.

43 F. L. de Panthou, E. Belorizky, R. Calemczuk, Luneau, D. C. Marcenat, E. Ressouche, P. Turek, P. Rey, *J. Am. Chem. Soc*. 1995, **117**, 11247.

44 V. I. Ovcharenko, S. V. Fokin, G. V. Romanenko, Y. G. Shvedenkov, V. N. Ikorskii, E. V. Tretyakov, S. F. Vasilevskii, *J. Struct. Chem*. 2002, **43**, 153.

45 D. C. Johnston, M. Troyer, S. Miyahara, D. Lidsky, K. Ueda, M. Azuma, Z. Hiroi, M. Takano, M. Isobe, Y. Ueda, M. A. Korotin, V. I. Anisimov, A. V. Mahajan, L. L. Miller, Los Alamos National Laboratory, Preprint Archive, Condensed Matter; Los Alamos National Laboratory: Los Alamos, NM, 2000; 1-63, arXiv:con-mat/0001147.

46 M. Troyer, H. Tsunetsugu, D. Würtz, *Phys. Rev. B* 1994, **50**, 13515.

47 O. Kahn, "Molecular Magnetism", VCH, New York, 1993.

48 J. B. Goodenough, *Phys. Rev*. 1955, **100**, 564.

49 J. Kanamori, *J. Phys. Chem. Solids* 1959, **10**, 87.

50 P. W. Anderson, Chapter 2 (p.25-83), in Magnetism, edited by Rado, G.T. and Suhl, H. (Academic Press, New York, 1963).

51 A. Escuer, E. Peñalba, R. Vicente, X. Solans. M. Font-Bardía, *J. Chem. Soc., Dalton Trans*. 1997, 2315.

52 M. Rodríguez, A. Llobet, M. Corbella, P. Müller, M. A. Usón, A. E. Martell, J. Reibenspies, *J. Chem. Soc., Dalton Trans*. 2002, 2900.

53 F. W. B. Einstein, A. C. Willis, *Inorg. Chem*. 1981, **20**, 609.